

# Detection of Silver Ions Using Dielectrophoretic Tweezers-Based Force Spectroscopy

Seungyeop Choi,<sup>†</sup> Gyudo Lee,<sup>†,‡</sup> In Soo Park,<sup>†</sup> Myeonggu Son,<sup>†</sup> Woong Kim,<sup>§</sup> Hyungbeen Lee,<sup>†</sup> Sei-Young Lee,<sup>†</sup> Sungsoo Na,<sup>||</sup> Dae Sung Yoon,<sup>⊥</sup> Rashid Bashir,<sup>#</sup> Jinsung Park,<sup>\*,§</sup> and Sang Woo Lee<sup>\*,†</sup>

<sup>†</sup>Department of Biomedical Engineering, Yonsei University, Wonju 26493, Republic of Korea

<sup>‡</sup>School of Public Health, Harvard University, Boston, Massachusetts 02115, United States

<sup>§</sup>Department of Control and Instrumentation Engineering, Korea University, Sejong 30019, Republic of Korea

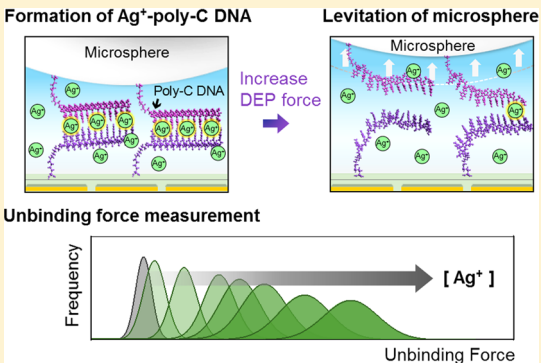
<sup>||</sup>Department of Mechanical Engineering, Korea University, Seoul 02841, Republic of Korea

<sup>⊥</sup>Department of Bio-convergence Engineering, Korea University, Seoul 02841, Republic of Korea

<sup>#</sup>Department of Bioengineering, University Illinois at Urbana–Champaign, Urbana, Illinois 61801, United States

## Supporting Information

**ABSTRACT:** Understanding of the interactions of silver ions ( $\text{Ag}^+$ ) with polynucleotides is important not only to detect  $\text{Ag}^+$  over a wide range of concentrations in a simple, robust, and high-throughput manner but also to investigate the intermolecular interactions of hydrogen and coordinate interactions that are generated due to the interplay of  $\text{Ag}^+$ , hydrogen ions ( $\text{H}^+$ ), and polynucleotides since it is critical to prevent adverse environmental effects that may cause DNA damage and develop strategies to treat this damage. Here, we demonstrate a novel approach to simultaneously detect  $\text{Ag}^+$  satisfying the above requirements and examine the combined intermolecular interactions of  $\text{Ag}^+$ –polycytosine and  $\text{H}^+$ –polycytosine DNA complexes using dielectrophoretic tweezers-based force spectroscopy. For this investigation, we detected  $\text{Ag}^+$  over a range of concentrations (1 nM to 100  $\mu\text{M}$ ) by quantifying the rupture force of the combined interactions and examined the interplay between the three factors ( $\text{Ag}^+$ ,  $\text{H}^+$ , and polycytosine) using the same assay for the detection of  $\text{Ag}^+$ . Our study provides a new avenue not only for the detection of heavy metal ions but also for the investigation of heavy metal ions–polynucleotide DNA complexes using the same assay.



The diagram illustrates the experimental setup and results. It is divided into three main sections: 1. Formation of  $\text{Ag}^+$ –poly-C DNA: A microsphere is shown with poly-C DNA strands attached to its surface. Silver ions ( $\text{Ag}^+$ ) are shown binding to the DNA. 2. Levitation of microsphere: An arrow labeled 'Increase DEP force' points to a second diagram where the microsphere is levitated, pulling the DNA strands away from the surface. 3. Unbinding force measurement: A graph plots Frequency on the y-axis and Unbinding Force on the x-axis. A series of overlapping green curves represent the unbinding force distribution at different concentrations of  $\text{Ag}^+$ . An arrow labeled  $[\text{Ag}^+]$  indicates that as the concentration increases, the unbinding force distribution shifts to the right, indicating higher rupture forces.

Silver has been used as an antimicrobial agent for at least six millennia.<sup>1</sup> Ancient Egyptians, Greeks, and Romans used silver containers to keep liquid fresh and silver pads to heal wounds.<sup>2</sup> Recent advances in nanotechnology have resulted in the production of silver nanomaterials with improved antimicrobial activity, generating many reports of silver biocidal products.<sup>3</sup> However, there have still been concerns over the environmental and health safety risks posed by silver ions ( $\text{Ag}^+$ ) if they were released from these products into various ecosystems.<sup>4</sup> Many studies have shown that  $\text{Ag}^+$  can adversely affect wildlife<sup>5–7</sup> and even humans.<sup>8</sup> Furthermore, released  $\text{Ag}^+$  may cause DNA damage through the formation of  $\text{Ag}^+$ –polynucleotide complexes.<sup>9</sup> Therefore, it is important to develop sensitive methods to detect the release of  $\text{Ag}^+$  into the environment and investigate the formation of  $\text{Ag}^+$ –polynucleotide complexes.

Some attempts have been made to detect  $\text{Ag}^+$  using atomic absorption spectrometry<sup>10</sup> and fluorescent probes based on the binding specificity between metal ions and organic molecules.<sup>11–13</sup> However, these approaches are time-consuming and not sensitive enough to detect low  $\text{Ag}^+$  concentrations. Alternatively, detection methods utilizing cytosine (C)-

containing polynucleotides have been demonstrated with high selectivity and specificity of C-rich DNA for  $\text{Ag}^+$  detection in fluorescence-based assays (10 nM to 1  $\mu\text{M}$ ),<sup>14–18</sup> electrochemical sensors (10 nM to 10  $\mu\text{M}$ ),<sup>19–21</sup> resonant cantilevers (1 nM to 10  $\mu\text{M}$ ),<sup>22</sup> and Kelvin probe force microscopy (100 pM to 100 nM).<sup>23</sup> Although these techniques offer higher sensitivities for  $\text{Ag}^+$  detection than conventional methods, they still have limitations in the investigation of combined interactions mediated by hydrogen ( $\text{H}^+$ –polynucleotide) and coordinate ( $\text{Ag}^+$ –polynucleotide) complexes<sup>14,24–26</sup> that are critically related to generate  $\text{Ag}^+$ –polynucleotide complexes. Therefore, a method for the detection  $\text{Ag}^+$  over a wide range of concentrations using a simple and high-throughput technique as well as the investigation of the combined intermolecular interactions generated by the interplay of  $\text{Ag}^+$ , hydrogen ions ( $\text{H}^+$ ), and polynucleotides is required. The rupture force of the combined interactions as a probe is a possible candidate to

Received: January 10, 2016

Accepted: July 7, 2016

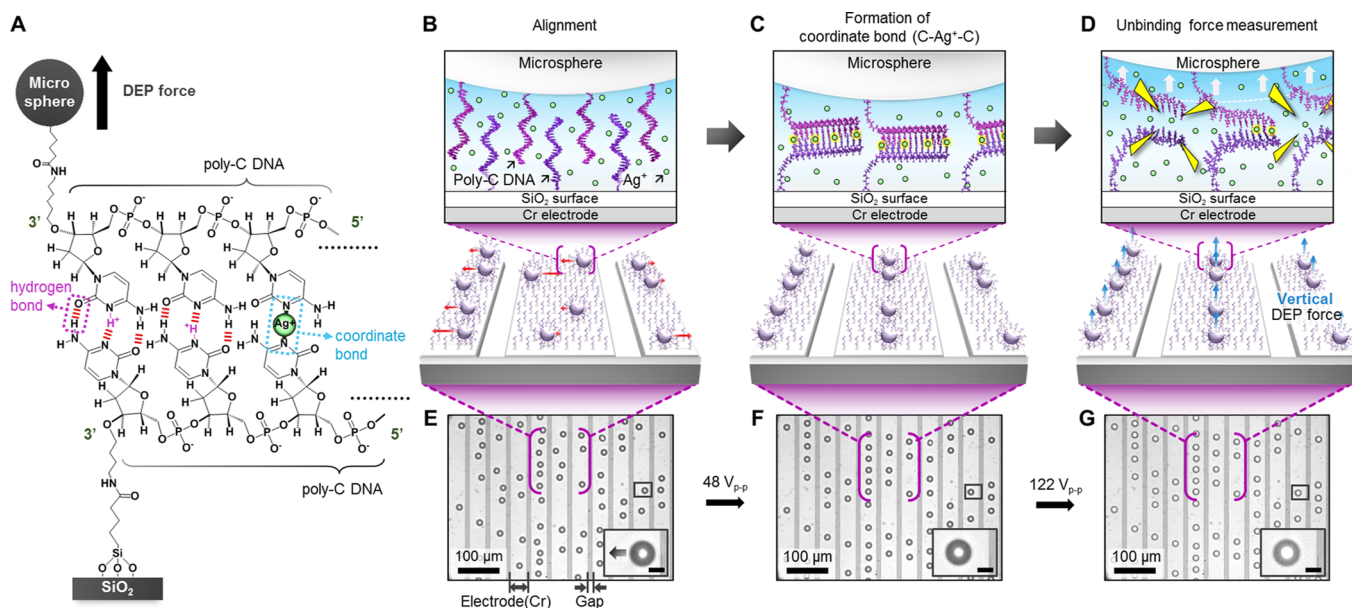


**Figure 1.** Overview of the measurement system. (A) Schematic (not drawn to scale) outlining the DEPFS to measure interactions between parallel poly-C DNA mediated by  $\text{Ag}^+$ . The inherent forces in  $\text{H}^+/\text{Ag}^+$ -poly-C complexes, with the combination of hydrogen and coordinate bonds, can be assessed by an upward movement of a microsphere due to the DEP force. (B–D) Schematic illustration of the experimental configuration where the details are provided in the main text. The measurement procedure involved three steps. (B) The first step was to apply a negative DEP force ( $48 \text{ V}_{\text{p-p}}$ , 1 MHz) to trap the microspheres with immobilized poly-C DNA on the center of the electrode. (C) The next step was to induce a C– $\text{Ag}^+$ –C bond between the microsphere probe and silicon dioxide ( $\text{SiO}_2$ ) surface. (D) Then, the rupture force was measured using a vertical DEP force ( $122 \text{ V}_{\text{p-p}}$ , 1 MHz). (E–G) Optical images obtained following the (B–D) steps with an  $\text{Ag}^+$  concentration of 100 pM ( $100 \mu\text{m}$  scale bar) in a DEP chip with interdigitated electrodes. The inset shows single microsphere movements for each applied voltage ( $10 \mu\text{m}$  scale bar). The negative DEP principle and the fabrication method of the chip are described in the [Materials and Methods](#) section and the [Supporting Information](#).

satisfy these requirements. Nevertheless, a quantitative analytical approach has not been reported to date.

Dielectrophoretic-tweezers based force spectroscopy (DEPFS), which has been developed recently and used inside microfluidic devices,<sup>27–33</sup> enables the measurement of numerous intermolecular interactions such as various weak binding interactions under various pH conditions, specific ligand–receptor binding, nonspecific interactions, and DNA–DNA interactions, by simultaneously using hundreds of chemically or biological functionalized microspheres as probes in a given environment. As a result, DEPFS can be used to obtain statistically reliable data of unbinding intermolecular interactions and this data can be utilized to statistically investigate the properties of the interactions in a simple, robust, and high-throughput manner, as opposed to other force spectroscopic approaches. Herein, by the use of the DEPFS approach, we present a novel method that enables not only highly sensitive detection of  $\text{Ag}^+$  over a wide range of concentrations but also quantitative investigation of the interplay between  $\text{Ag}^+$ ,  $\text{H}^+$ , and polycytosine (poly-C) DNA based on exploring the intermolecular forces of  $\text{Ag}^+/\text{H}^+$  poly-C DNA complexes. Using this approach, we measured the unbinding (rupture) force ( $F_{\text{U}}$ ) in DNA complexes over a wide detection range from 100 pM to 100  $\mu\text{M}$   $\text{Ag}^+$  in pure water and drinking water samples. Moreover, our force spectroscopy method was used for the statistical evaluation of cooperativity in coordinate interactions of  $\text{Ag}^+$ -poly-C DNAs and hydrogen interactions of  $\text{H}^+$ -poly-C DNAs within  $\text{Ag}^+/\text{H}^+$  poly-C DNA complexes, which allows us to investigate the  $\text{Ag}^+$  interaction mechanism within DNA polynucleotides.

## MATERIALS AND METHODS

**Fabrication of a Microfluidic Chip.** The interdigitated electrode array pattern ( $40 \mu\text{m}$  wide and  $10 \mu\text{m}$  separations) was fabricated on an oxidized silicon wafer (i-Nexus, Seongnam, Republic of Korea) using photolithography techniques. A  $1000 \text{ \AA}$  thick chromium interdigitated electrode array pattern was deposited on the substrate using the thermal evaporator technique and standard lift-off process. The metal electrodes were covered by a  $7000 \text{ \AA}$  thick plasma-enhanced chemical vapor deposited (PECVD) silicon dioxide. The top view of the structure is imaged in [Figure 1E–G](#), and the schematic cross-section view of the chip is described in [Figure N2](#).

**Preparation of Oligonucleotide.** Poly-C DNA was obtained with commercial DNA sequencing services (Cosmogentech, Seoul, Republic of Korea). Poly-C DNA has the following sequences: 24-base poly-C DNA ( $5'$ -CCC CCC CCC CCC CCC CCC CCC- $3'$ -( $\text{CH}_2$ )<sub>6</sub>- $\text{NH}_2$  and 6-FAM- $5'$ -CCC CCC CCC CCC CCC CCC CCC CCC- $3'$ -( $\text{CH}_2$ )<sub>6</sub>- $\text{NH}_2$ ); 12-base poly-C DNA ( $5'$ -CCC CCC CCC CCC- $3'$ -( $\text{CH}_2$ )<sub>6</sub>- $\text{NH}_2$ ); 6-base poly-C DNA ( $5'$ -CCC CCC- $3'$ -( $\text{CH}_2$ )<sub>6</sub>- $\text{NH}_2$ ). All oligonucleotide at the high-pressure liquid chromatography purity were synthesized and used for functionalization of both surfaces of DEP chip and microsphere.

**Functionalization of the Microfluidic Device by Poly-C DNA.** The surface of the fabricated device was functionalized as follows: poly-C DNA was immobilized on the surface of the device with a carboxyl-terminated oxide surface layer by 3-triethoxysilylpropyl succinic anhydride (TESPSA).<sup>34</sup> The silicon dioxide chip was first transferred to a solution consisting of  $\text{H}_2\text{SO}_4$ – $\text{H}_2\text{O}_2$  (1:2), resulting in a hydroxyl functionalized

substrate ( $\text{SiO}_2\text{-OH}$ ). This hydroxyl-functionalized substrate was then immersed in 100 mM TESPSA (Gelest, Morrisville, PA) in an organic solvent (toluene, 99.8%) overnight ( $\text{SiO}_2\text{-COOH}$ ). The carboxylated substrate was cleaned with three different solvents (toluene, *N,N*-dimethylformamide (DMF, Sigma-Aldrich, St. Louis, MO; 99.9% HPLC grade), and distilled water) and dried by nitrogen, and then the carboxylated substrate was immersed in 65 mM *N*-(3-dimethylaminopropyl)-*N'*-ethylcarbodiimide hydrochloride (EDC; Sigma-Aldrich, 99%) and 108 mM *N*-hydroxysuccinimide (NHS; Sigma-Aldrich, 98%) in 0.01 M phosphate-buffered saline (PBS) (Gibco, Gaithersburg, MD) at a pH of 7.2 for 1 h. Each of 200, 400, and 800 nM poly-C DNA solutions were then added to this solution to form amide bond with chip surface during overnight ( $\text{SiO}_2\text{-poly-C DNA}$ ). After poly-C DNA immobilization, the DEP chip substrate was rinsed with an excess PBS buffer solution and a distilled water solution and then dried with nitrogen gas. All sample preparations were performed at 22 °C.

**Preparation of the Microspheres with Immobilized Poly-C DNA.** To prepare the microspheres immobilized with poly-C DNA, 3 mg/mL of carboxylated polystyrene microspheres (Kisker, Steinfurt, Germany; 15  $\mu\text{m}$ ) was reacted with 6.25 mg of 99% EDC and 6.25 mg of 98% NHS in PBS (Gibco; 0.01 M, pH 7.2) for 1 h. The reaction mixture was then incubated with 1  $\mu\text{M}$  poly-C DNA overnight. The resulting microspheres with immobilized poly-C DNA were vortexed and rinsed five times in PBS by centrifugation. The microspheres were diluted with distilled water (Gibco, Gaithersburg, MD) or drinking water (Jeu Samdasoo, JPDC, and Republic of Korea) and centrifuged before use. All sample preparations were performed at 22 °C.

**Characterization Method of the Functionalized Chip and Microsphere by Fluorescence Microscopy, Scanning Electron Microscopy (SEM), and Atomic Force Microscopy (AFM).** The microsphere and DEP chip substrate immobilized with poly-C DNA were washed with PBS and distilled water prior to the analysis. The surfaces of the microspheres and plasma enhanced chemical vapor deposition (PECVD) oxide were examined by fluorescence microscopy (BX60, Olympus, Tokyo, Japan) using a WB filter. Field emission SEM (JSM-7001F, JEOL, Tokyo, Japan) was used to observe the morphology and composition of the polystyrene microsphere surface, where poly-C DNA and carboxyl functional groups were immobilized. Because the microspheres with immobilized poly-C DNA and carboxylated polystyrene microspheres are nonconducting materials, the samples were preprocessed by platinum ion sputtering to provide protection from electron damage. The contrast of the top-view SEM images (Figure S2) was analyzed using ImageJ. AFM measurements were performed using a Multimode V (Veeco, Santa Barbara, CA) in air and the images ( $5 \times 5 \mu\text{m}^2$ ) were further analyzed using Nanoscope software (Bruker). The AFM height images for the DEP chip substrate with or without poly-C DNA were quantified by comparing the surface roughness defined as the root mean squared value:

$$R_q = \sqrt{(1/n) \sum_{i=1}^n y_i^2}$$

**Measurement Methods of the Unbinding Force in the C-Ag<sup>+</sup>-C/C-H<sup>+</sup>-C Complex.** The polydimethylsiloxane (PDMS) chamber, which was approximately  $6 \times 6 \times 1.2$

mm<sup>3</sup> with a 3 mm diameter hole in the middle, was put into contact with the DEP chip surface functionalized immobilized poly-C DNA. A mixture of the microspheres with immobilized poly-C DNA with metal ions (9:1; 10  $\mu\text{L}$ ) was injected into the PDMS chamber. All metal ion solutions were used with metal nitrates salts ( $\text{AgNO}_3$ ,  $\text{LiNO}_3$ ,  $\text{NaNO}_3$ ,  $\text{Hg}(\text{NO}_3)_2$ ,  $\text{Zn}(\text{NO}_3)_2$ , and  $\text{Fe}(\text{NO}_3)_3$ ; Sigma-Aldrich). An ac voltage was applied to the electrodes in the microfluidic chip using a WMA300 amplifier (Falco Systems, Amsterdam, The Netherlands) connected to a 33250 function generator (Agilent Technologies, Santa Clara, CA), and the applied voltages was rechecked with an oscilloscope (WaveRunner 6050, LeCroy, New York, NY) for the verification. The bead movement was recorded by a top-view charge coupled device camera (Motionscope M3, Redlake, San Diego, CA). The unbinding force ( $F_U$ ) of the molecular interactions was quantified by using a combination of the grayscale variation method and DEP force maps acquired from finite elements simulation (FES).<sup>29</sup> The detail method is described in the Supporting Information, Note 1. Briefly, to determine the ruptured point of microspheres (probes) from the chip substrate surface, we used the grayscale values from the inner region of each microsphere in a top-view optical image as a function of applied voltage.<sup>29</sup> For the characterization of DEP forces exerted on a microsphere, well-established FES results were used, albeit a few attempts so far to depict the DEP force map by using optical tweezers.<sup>35–37</sup>

**Calibration of DEP Chip.** Although the DEP chips were made through the same MEMS fabrication process, the chips often show difference performance. Hence we check the quality of DEP chips before use of them. We provide our results regarding chip performance (Figure S4), where we used carboxylated microspheres and well-cleaned chip, showing the similar performance of 20 chips regarding the unbinding voltage measurement. The mean unbinding voltage, 1.002 V<sub>p-p</sub> corresponds to DEP force, 46.51 pN, which is within range of van der Waals interaction (cf., the gravity of the microsphere (~0.1 pN)).

## RESULTS

**Principle of DEPFS for the Measurement of the Interactions of Ag<sup>+</sup>/H<sup>+</sup> Poly-C DNA Complexes.** Our aim was to directly and massively measure the force in C-Ag<sup>+</sup>-C/C-H<sup>+</sup>-C as a function of the Ag<sup>+</sup> concentration using a negative DEP (nDEP) force<sup>38</sup> in microspheres (probes) containing functionalized poly-C DNA (Figure 1 and Supporting Information, Note 1). To measure the intermolecular interactions of Ag<sup>+</sup>/H<sup>+</sup> poly-C DNA complexes, we functionalized poly-C DNA on hundreds of polystyrene microspheres and a DEP chip substrate ( $\text{SiO}_2$ ) (Figure 1A and Figure S1). The microspheres interacted with the poly-C DNA functionalized surface on the chip substrate with or without Ag<sup>+</sup>, resulting in the formation of intermolecular interactions between two surfaces (i.e., the microspheres and chip substrate). Because we immobilized the poly-C DNA onto two different surfaces (i.e., microspheres and DEP chip) using a 3' amine group, we supposed that in our configuration the unzipping mode is prevalent, rather than the shear mode (Figure S5).<sup>39</sup>

As the DEP force increased, such interactions were broken due to the upward movement of the microspheres with immobilized poly-C DNA from the chip substrate, which allows us to directly measure the intermolecular (unbinding) forces between poly-C DNA mediated by Ag<sup>+</sup> and H<sup>+</sup>. Specifically, the

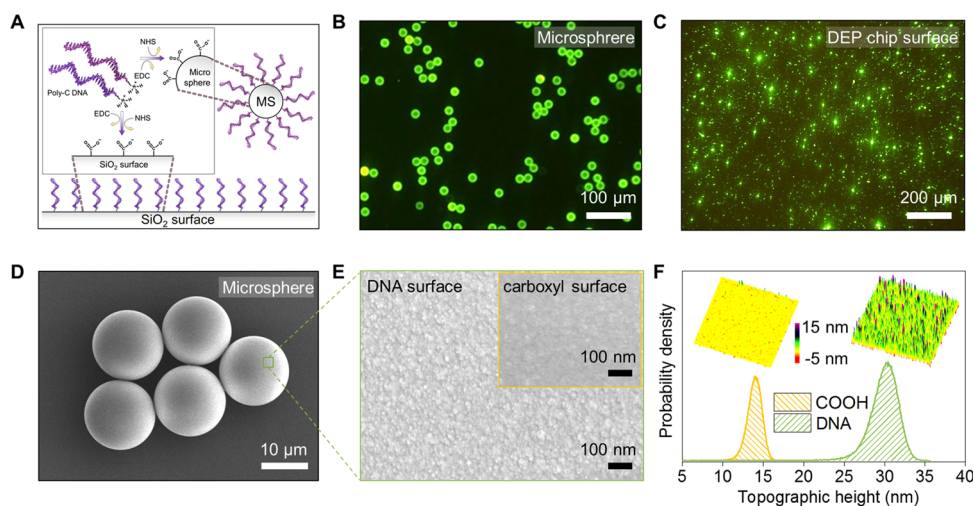


**Figure 2.** Surface immobilization and characterization of poly-C DNA. (A) Schematic illustration of poly-C DNA covalent binding on the SiO<sub>2</sub> surface and the microspheres with EDC/NHS. (B,C) Fluorescence images of the microspheres with immobilized poly-C DNA (B) and the DEP chip surface (C) labeled with 6-FAM (excitation/emission wavelengths of 495 nm/520 nm). (D) SEM image of the microspheres with immobilized poly-C DNA. (E) The image of the boxed region in part D where poly-C DNA can be clearly seen. The inset shows an SEM image of the surface of carboxylated polystyrene microspheres. (F) Topographic height distribution obtained from the AFM image. The inset shows AFM images of the carboxylated DEP chip surface (left) and poly-C DNA-immobilized DEP chip surface (right) where each image size is 5 × 5 μm<sup>2</sup>. The scale bars are (B) 100 μm, (C) 200 μm, (D) 10 μm, and (E) 100 nm.

microspheres were randomly distributed on the silicon dioxide film over an interdigitated (IDT) electrode within a microfluidic chamber. When an ac voltage (48 V<sub>p-p</sub>, 1 MHz) was applied to the IDT electrode, the microspheres were aligned along the center of the electrode by the nDEP force (Figure 1B), and then they interacted with Ag<sup>+</sup>, resulting in the formation of C–Ag<sup>+</sup>–C and C–H<sup>+</sup>–C complexes (Figure 1C). A higher voltage (~122 V<sub>p-p</sub>, 1 MHz) applied to the IDT electrode could break the complexes when the microspheres were vertically levitated at the center of the electrode (Figure 1D). The microsphere movement and displacement were evaluated using optical microscopy images, where the microspheres brightness depended on the changes of the trap height due to the defocusing depth, which was quantitatively analyzed to determine the unbinding voltage of the complexes using a grayscale method (Figure 1E–G, see Materials and Methods).<sup>29</sup>

**Characterization of Both the Microspheres and DEP Chip Substrate with Immobilized Poly-C DNA.** To obtain poly-C DNA immobilized on microspheres and DNA-coated chips, amino-labeled poly-C DNA was immobilized on polystyrene microspheres, and the silicon dioxide substrate surface of the DEP chip, which were both functionalized with carboxyl groups via peptide bonds (Figure 2A and Figure S1). The detailed functionalization procedure is described in the Materials and Methods section. The fabrication of the microspheres and DEP chip substrates was verified by fluorescent microscopy (Figure 2B,C). The use of fluorescence-labeled oligonucleotide is very intuitive to see whether the functionalization protocol is working well or not.<sup>22</sup>

We have also used poly-C DNA labeled with fluorescence (6-FAM) to validate the functionalization of oligonucleotides not only on probe bead but also on the DEP chip surface, because the functionalization protocol of oligonucleotide is the same in both cases (Figure S1). When we perform the silver ion detection using DEPFS, however, we did not use those fluorescence-labeled oligonucleotides, rather we used pure oligonucleotide sequence without fluorescent dye molecules

(i.e., 6-FAM) to avoid experimental errors in force measurements deriving from the dye molecules.

Extra experiments (i.e., AFM and SEM) were produced to observe the distribution of immobilized poly-C DNA without fluorescence dye. We also examined the microspheres with immobilized poly-C DNA and DNA-coated chips using SEM and AFM, respectively (Figure 2D–F). Because the AFM analysis of the microspheres surface is perturbed by its curvature and wobbling (i.e., rocking motion) of microspheres,<sup>40–42</sup> we used SEM to examine not only the morphology of the microspheres with immobilized poly-C DNA but also their surface where poly-C DNA is observed as multiple tiny granules (several nanometers). This result is consistent with the results of a previous report that observed to increase the tendency of granularity in the presence of poly-C DNA.<sup>43</sup> By contrast, the control sample (carboxylated polystyrene microspheres) showed a relatively flat surface (inset of Figure 2E and Figure S2).

We have used AFM to probe topographic change of the chip surface on which biomolecules (here, poly-C DNA) are functionalized.<sup>44,45</sup> To quantify such a topographic profile change, the histogram of surface roughness has been used to compare before and after step of the immobilization of poly-C DNA. Because (the size of) the oligonucleotide is larger than carboxyl functional groups, the height distribution of the surface where DNA are immobilized would become higher. This shows that the height difference in histogram shows huge shift from left to right under the same AFM imaging conditions (as shown in Figure 2F). Generally, DNA-immobilization makes the surface roughness higher,<sup>46</sup> showing a larger width of the histogram of topographic height, rather than surface roughness in the absence of DNA (Figure S3).

Through these various microscopy analyses, we confirmed the basic fabrication method, but this does not guarantee the stability of the microspheres with immobilized poly-C DNA of this system. Moreover, it is well-known that tensional forces or intermolecular interactions between DNAs are dependent on the DNA length as well as microenvironments such as

temperature or pH,<sup>47–50</sup> as are the hydrogen and coordinate interactions generated by the interplay between  $\text{Ag}^+$ ,  $\text{H}^+$ , and poly-C DNA. Therefore, further optimization is required, as described below.

**Optimization of Microspheres for the Interactions of  $\text{Ag}^+/\text{H}^+$  Poly-C DNA Complexes.** It has been reported that hydrogen bond can occur between a cytosine and hemiprotonated cytosine ( $\text{C}-\text{H}^+-\text{C}$ ) under weak acidic conditions (pH 5).<sup>39,51</sup> The  $\text{C}-\text{H}^+-\text{C}$  hydrogen bond can also be replaced by coordinative bonds to  $\text{Ag}^+$  through the bridge between hetero nitrogen atoms in each cytosine (i.e., becoming  $\text{C}-\text{Ag}^+-\text{C}$ ) when  $\text{Ag}^+$  is in the solution.<sup>52</sup> Hence, the length of poly-C DNA ( $L$ ) needs to be optimized in order to make the best. The microspheres with immobilized poly-C DNA for highly accurate measurement of the interactions of  $\text{Ag}^+/\text{H}^+$  poly-C DNA complexes.

For the optimization of the microspheres with immobilized poly-C DNA, we measured  $F_U$  between the microspheres and the chip surface, which were functionalized with different lengths ( $L$ ) of poly-C DNA in either the presence or absence of  $\text{Ag}^+$  in distilled water (pH 5.4) using DEPFS. As expected, a larger  $F_U$  was obtained as  $L$  increased because of either the increment of the number of hemicytosinium duplexes to form  $\text{C}-\text{H}^+-\text{C}$  without  $\text{Ag}^+$  or the combination of hemicytosinium duplexes and coordinate duplexes to form  $\text{C}-\text{Ag}^+-\text{C}$  with  $\text{Ag}^+$  (Figure 3A,B). Naturally, the  $F_U$  value with  $\text{Ag}^+$  is greater than that without  $\text{Ag}^+$  since the coordinate interaction has a higher binding strength than the hydrogen interaction.<sup>39</sup> It is also shown that the poly- $\text{C}_6$  DNA resulted in a very small  $F_U$  value without  $\text{Ag}^+$ . This may be due to the thermodynamic instability of DNA hybridization in the case of shorter double-stranded

DNA at room temperature,<sup>25,53</sup> and this instability can be stabilized by the coordinate bonds when  $\text{Ag}^+$  is introduced (Figure 3B). The mean unbinding force ( $\langle F_U \rangle$ ) was summarized from the measured  $F_U$  data and is plotted in Figure 3C. Interestingly, it was found that the difference ( $S_F$ ) between  $\langle F_U \rangle$  in the absence or presence of  $\text{Ag}^+$  was saturated at  $\text{C}_{24}$  (Figure 3D). This implies that 24-base poly-C DNA ( $\text{C}_{24}$ ) is large enough to detect  $10 \mu\text{M}$   $\text{Ag}^+$ . This saturation phenomenon of  $\langle F_U \rangle$  at  $\text{C}_{24}$  can be explained by two possible scenarios: (i) the interaction between poly-C DNAs is thermodynamically stabilized at  $L = 24$  and (ii)  $\langle F_U \rangle$  is saturated at a certain  $L$  (here, 24-base) because of the unzipping mode (in unbinding behavior) of hybridized DNA molecules.<sup>54</sup> Together, we chose poly- $\text{C}_{24}$  DNA and applied it in all experiments.

**Measurements of the Interactions of  $\text{Ag}^+/\text{H}^+$  Poly-C DNA Complexes.** To measure the interactions of  $\text{Ag}^+/\text{H}^+$  poly-C DNA complexes mediated by hydrogen ( $\text{C}-\text{H}^+-\text{C}$ ) and coordinate ( $\text{C}-\text{Ag}^+-\text{C}$ ) interactions using DEPFS, we introduced  $\text{Ag}^+$  into the microfluidic chip between the microspheres with immobilized poly-C DNA and chip substrate. Before the measurement of this interaction, we measured the conductivity of the medium containing different  $\text{Ag}^+$  concentrations (100 pM to 1 mM) because conductivity is an important parameter for DEPFS.<sup>55,56</sup> We found that the  $\text{Ag}^+$  concentrations tested, except for the highest value (1 mM), did not significantly influence the medium conductivity (Figure S6). We further validated the effect of the  $\text{Ag}^+$  concentration on the medium conductivity by measuring  $\langle F_U \rangle$  with different  $\text{Ag}^+$  concentrations using carboxylated microspheres and a negatively charged surface, which showed similar results. On the basis of these findings, we measured the interactions of  $\text{Ag}^+/\text{H}^+$  poly-C DNA complexes in the range of 100 pM to 100  $\mu\text{M}$   $\text{Ag}^+$ , where the results are shown in Figure S7. The  $\langle F_U \rangle$  of the interaction increased with increasing  $\text{Ag}^+$  concentration from  $12.51 \pm 1.33$  nN to  $35.75 \pm 3.20$  nN (Figure S7).

## DISCUSSION

In order to analyze the detection capability of  $\text{Ag}^+$  using DEPFS, which evaluates the potential of the  $\text{Ag}^+$  sensor, we plotted the mean rupture force ( $\langle F_U \rangle$ ) and standard deviation using the  $F_U$  data (Figure 4A). As shown in Figure 4A,  $\langle F_U \rangle$  linearly increased with increasing  $\text{Ag}^+$  concentration in the semilogarithm scale. More than 400 microspheres with immobilized poly-C DNA on multiple DEP chips were used in this analysis, which demonstrates a high reliability ( $P < 0.0001$ ) and a very short detection time ( $< 3$  min). The limit of detection was  $\sim 300$  pM (Figure S8), which is not an overwhelming value but pretty good by comparison with conventional methods such as stripping voltammetry at a chemically modified electrode ( $\sim 2$  pM),<sup>57</sup> and inductively coupled plasma-mass spectrometry ( $\sim 6$  pM).<sup>58</sup>

We also evaluated the ion selectivity using various metal ions (100 nM) including  $\text{Zn}^{2+}$ ,  $\text{Li}^+$ ,  $\text{Na}^+$ ,  $\text{Hg}^{2+}$ , and  $\text{Fe}^{3+}$  (Figure 4B). To quantify the detecting ability of our DEPES, we calculate the selectivity coefficient ( $\xi$ ) defined as the ratio of the two equilibrium constants between poly-C DNA and either  $\text{Ag}^+$  or other cations ( $X$ ) (i.e.,  $\xi = K_{\text{DNA},X}/K_{\text{DNA},\text{Ag}^+}$ ) (see the Supporting Information, note 4 in detail). It is shown that  $\text{Ag}^+$  is quite selective in our DEPFS system, at least 25% more rather than other cations, which demonstrated good selectivity in capturing  $\text{Ag}^+$  compared to other metal ions.

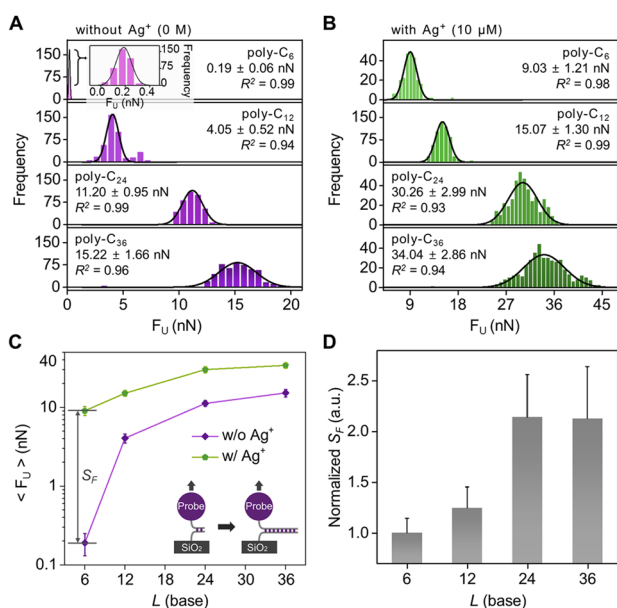


**Figure 3.** Quantification of the intermolecular forces between  $\text{Ag}^+$ ,  $\text{H}^+$ , and poly-C DNA with different lengths ( $L$ ) ranging from 6-base to 36-base. (A,B) Unbinding force ( $F_U$ ) histograms and Gaussian fits with/without  $\text{Ag}^+$  for different  $L$  values. (C) Mean unbinding force ( $\langle F_U \rangle$ ) and standard deviations acquired from parts A and B. The inset depicts an illustration of the unzipping of DNA molecules. (D) The shift force ( $S_F$ ) is the difference of the  $\langle F_U \rangle$  values obtained with and without  $\text{Ag}^+$ , which was obtained from normalization of the  $S_F$  values by the  $S_F$  value of poly- $\text{C}_6$  DNA.

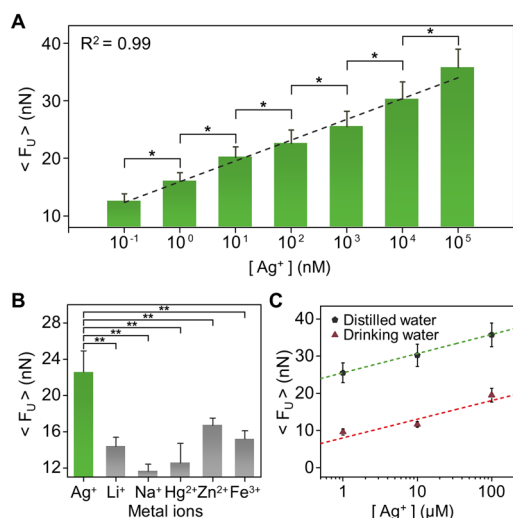


**Figure 4.** Quantitative characterization of the detection capability of  $Ag^+$  using DEPFS. (A) The mean rupture force ( $\langle F_U \rangle$ ) and standard deviation are obtained from a  $Ag^+$  assay with DEPFS in the semilogarithmic scale. The student's  $t$  test (two-tailed) was used for statistical analysis ( $*P < 0.0001$ ). The dashed line was fit by the following logarithmic function:  $\langle F_U \rangle = 3.65 \times 10^{-9} \times \log[Ag^+] + 48.91 \times 10^{-9}$ . (B) Ion selectivity test and (C) practical application of DEPFS for a  $Ag^+$  sensor ( $**P < 0.0001$ ).

To validate its performance as a robust practical device for  $Ag^+$  detection, we tested whether DEPFS could not only detect  $Ag^+$  but also measure its concentration in drinking water (Figure 4C). For this, we analyzed different concentrations of  $AgNO_3$  (1–100  $\mu M$ ) in natural drinking water (Jeju Samdasoo, JPDC, Republic of Korea). The results shown in Figure 4C reveal that the  $\langle F_U \rangle$  values in drinking water were about 20 nN lower than those in distilled water. We searched some factors to decrease  $\langle F_U \rangle$  values in drinking water. There are potentially many anions and organic compounds in drinking water. Some anions (bisulfite, borohydride etc.) can contribute to be low affinity between  $Ag^+$  and poly-C DNA through methylated cytosine<sup>59</sup> or reduction of silver ion.<sup>60</sup> Organic compounds (amino acids, peptides) also contribute to be low affinity between  $Ag^+$  and poly-C DNA because of a formation of  $Ag^+$ -thiolate clusters which have higher affinity than the  $C-Ag^+-C$  complex.<sup>61,62</sup> This tendency (reducing binding affinity of silver ions to DNA in drinking water) has been shown in previous studies.<sup>15,17,22,23</sup>

It should be also noted that the sensitivity and detection range of silver ions in drinking water are relatively poor rather than distilled water. One of the factors that influence the outcome may be attributed to the interferences between silver ions and poly-C DNA by other metal ions in drinking water. Although we focused on the comparison of intermolecular interaction of poly-C DNA in silver ions and other metal ions at the same concentration (i.e., 100 nM), it still remains unclear what kinds of or how the various metal ions interfere with the interaction between  $Ag^+$  and poly-C DNA. To understand this interference more clearly, it should need further investigation. Nevertheless,  $\langle F_U \rangle$  increased linearly with  $[Ag^+]$  in drinking water, suggesting that the DEPFS is suitable in practical applications to detect  $Ag^+$  in environmental waters based on the sensitivity requirement (46  $\mu M$ ) for standard drinking water stipulated by the U.S. Environmental Protection Agency.<sup>23</sup>

The linearity of  $\langle F_U \rangle$  in Figure 4A suggests that the interplay between  $Ag^+$ ,  $H^+$ , and poly-C can be described by a simple mechanistic model with hydrogen ( $C-H^+-C$ ) and coordinate ( $C-Ag^+-C$ ) interactions within  $Ag^+/H^+$  poly-C DNA complexes.<sup>63</sup> To investigate this suggestion, we calculated the individual bond-rupture force (i.e., a pair unbinding force of poly-C DNA) organizing  $Ag^+/H^+$  poly-C DNA complexes by Poisson statistics (Supporting Information, Note 3), utilizing the same  $\langle F_U \rangle$  measurement data (Figure 4A and Figure S7).

We assumed that force loading of contact area was equalized to all possible intermolecules from a statistical perspective, because the contact area between the microsphere and the electrode surface was symmetric geometry at the central point of contact area. Although the force loadings of intermolecules on the contact region are varied, average force loadings are maintained at a constant loading value. Also, we measured the mean force which represented the summation value of individual bonds and analyzed the single bond force using statistical method from average force. Even though individual intermolecules had various mix components of hydrogen and chelate bond, the single bond analyzed by the Poisson method represented the average bond probability of the poly-C complex mediated by metal ions from all possible bond compositions. With respect to the Poisson statistical model, the single unbinding force means the single molecule (i.e., a pair of DNA).<sup>64</sup>

Figure 5A shows that the individual bond-rupture force,  $F_{U\text{single}}$ , increased from 139 to 296 pN with increasing  $Ag^+$  concentration. The sigmoidal curve is also consistent with the results of a previous studies using DNA- $Ag^+$  interaction ( $C-Ag^+-C$ ).<sup>48,65</sup> This phenomenon is not observed when the

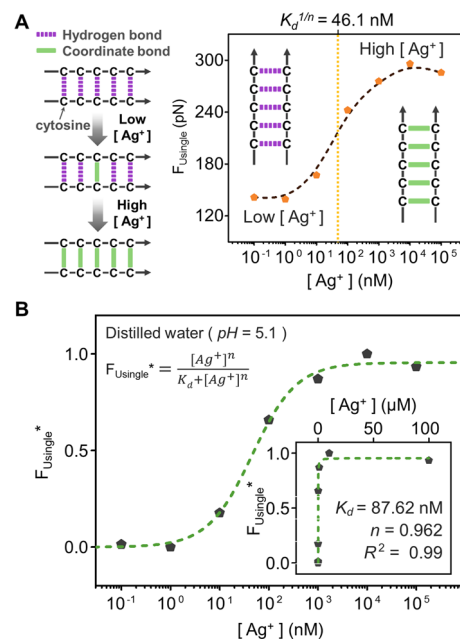


**Figure 5.** Statistical analysis of the interactions between  $Ag^+$  and poly-C DNA: (A) Schematic illustration of the interactions of  $H^+$  and  $Ag^+$  in the  $Ag^+$ -poly-C complex and single rupture forces of the  $Ag^+$ -poly-C complex interaction versus  $[Ag^+]$  in semilogarithmic scale. (B) Semilogarithmic plot of the normalized  $F_{U\text{single}}$  (i.e.,  $F_{U\text{single}}^*$ ) versus  $[Ag^+]$  (pentagon, black) fitted by the Hill equation (dashed line, green).  $F_{U\text{single}}^*$  is achieved by an equation as follows:  $F_{U\text{single}}^* = (F_{U\text{single}} - \text{MIN}[F_{U\text{single}}]) / (\text{MAX}[F_{U\text{single}}] - \text{MIN}[F_{U\text{single}}])$ . The inset depicts an arithmetic plot of part B.

individual intermolecular bond consists of one type of element. In addition, the individual bond-rupture force of the poly-C-DNA complex without  $\text{Ag}^+$ , in which hydrogen bond is created by hemiprotonated cytosine ( $\text{C}-\text{H}^+-\text{C}$ ) under weakly acidic conditions (pH 5),<sup>39,51</sup> remained constant at 128 pN even though the concentration of the poly-C-DNA complex was varied (Figure S11). Therefore, the increment of  $F_{\text{Usingle}}$  could be attributed to the degree of heterogeneity consisting of  $\text{C}-\text{H}^+-\text{C}$  and the  $\text{C}-\text{Ag}^+-\text{C}$  duplex in the  $\text{Ag}^+$ -poly-C-DNA complex, as described in the schematic illustration of Figure 5A.

Although the base stacking provides the critical contribution to stabilize general DNA helix conformation (e.g., B-form DNA and noncoding RNA molecule),<sup>63</sup> a recent AFM force spectroscopy<sup>66</sup> shows that the force of base stacking is estimated to be  $\sim 2$  pN. Moreover, the several studies on intermolecular interaction between poly-C DNAs have suggested that stacking interactions between adjacent  $\text{C}-\text{H}^+-\text{C}$  pairs is weak.<sup>67,68</sup> This is why many studies so far highlight the specific hydrogen bond ( $\text{C}-\text{H}^+-\text{C}$ ) in interactions between poly-C DNAs. Specifically, in weak acidic condition, poly-C DNA is known to consist of parallel-stranded duplexes with other poly-C DNA due to the hydrogen bonding (i.e.,  $\text{C}-\text{H}^+-\text{C}$ ).<sup>39</sup> Thus, we think that the contribution of hydrogen bond (i.e.,  $\text{C}-\text{H}^+-\text{C}$ ) is more prevalent than base stacking interaction in our experiment.

In the low  $\text{Ag}^+$  concentration region (e.g., 0.1, 1, and 10 nM),  $\text{Ag}^+$  ions appear to not actively interact with poly-C DNA so that the formation of  $\text{C}-\text{Ag}^+-\text{C}$  rarely occurs in poly-C DNA, whereas  $\text{C}-\text{Ag}^+-\text{C}$  in the  $\text{Ag}^+/\text{H}^+$ -poly-C-DNA complexes is dominant in the high  $\text{Ag}^+$  concentration region (e.g., 1, 10, and 100  $\mu\text{M}$ ). For instance, at 1 nM  $\text{Ag}^+$ , the  $F_{\text{Usingle}}$  value is about 139 pN, which is very similar to the individual bond-rupture force of hydrogen bonds ( $\sim 128$  pN). At 100  $\mu\text{M}$   $\text{Ag}^+$ , the  $F_{\text{Usingle}}$  is about 2.1 times greater than the values obtained at low  $\text{Ag}^+$  concentrations. Moreover, in the high  $\text{Ag}^+$  concentration region, it is seen that the  $F_{\text{Usingle}}$  value is saturated. To further understand the calculated results, we studied the binding cooperativity between  $\text{Ag}^+$  and poly-C DNA using the Hill equation, which is commonly used to investigate the cooperativity among more than two different bond compositions.<sup>63</sup> Figure 5B shows the Hill equation fit relative to the normalized value obtained using the data in Figure 5A. Our Hill equation is fitted from normalized  $F_{\text{Usingle}}$  (i.e.,  $F_{\text{Usingle}}^*$ ) (Figure 5A, caption). According to the classical theory of cooperativity between biomolecules, the binding affinity is characterized by the dissociation constant ( $K_d$ ) and Hill (cooperativity) coefficients ( $n$ ) in the Hill equation ( $R^2 = 0.99$ ). The values of  $K_d$  and  $n$  are 87.6 nM and 0.962, respectively, indicating not only that the  $\text{C}-\text{Ag}^+-\text{C}$  interaction has a higher specificity than nonspecific metal-ligand interactions, but surprisingly it is based on no cooperativity (i.e.,  $n \approx 1$ ). These values are in agreement with a previous study which analyzed that  $\text{Ag}^+$  specifically bound with the C:C base pair at a 1:1 molar ratio using isothermal titration calorimetry.<sup>69,70</sup>

In this work, the sigmoidal curve (Figure 5A) can be attributed to the combination ratio of hydrogen and coordinate bonds during the interplay between  $\text{Ag}^+$ ,  $\text{H}^+$ , and poly-C DNA. In other words, at low  $\text{Ag}^+$  concentrations, hydrogen bonding (i.e., the form of  $\text{C}-\text{H}^+-\text{C}$ ) is dominant, arising from the rare occurrence of the interplay between  $\text{Ag}^+$  and poly-C DNA. However, with increasing  $\text{Ag}^+$  concentration, it is transformed into a stronger interaction, administrated by  $\text{Ag}^+$ -mediated coordinate bonds since a critical concentration point exists (i.e.,

$K_d^{1/n} = 46.1$  nM). It is interesting that such a transformation ( $\text{C}-\text{H}^+-\text{C} \rightarrow \text{C}-\text{Ag}^+-\text{C}$ ) is determined not only by  $\text{Ag}^+$  concentration but also by the amount of hydrogen bonding, albeit with noncooperative binding. This may be due to the  $\text{Ag}^+$ -driven structural distortion of DNA molecules. Specifically, in the absence of  $\text{Ag}^+$ , poly-C DNA is formed as a parallel strand of the  $\text{C}-\text{H}^+-\text{C}$  duplex, which is symmetric, whereas, in the presence of  $\text{Ag}^+$ , the  $\text{C}-\text{Ag}^+-\text{C}$  duplex prefers an asymmetric structure due to  $\text{NH}_2 \cdots \text{O}=\text{C}$  intermolecular hydrogen bonds.<sup>52</sup> Such an asymmetry could perturb the intercalation of  $\text{Ag}^+$  between poly-C DNAs until the  $\text{Ag}^+$  concentration exceeds a certain critical concentration (in our case, 46.1 nM). This behavior may also be impacted by the DNA sequence and corresponding micro environments<sup>49</sup> or conformation.<sup>48</sup> Furthermore, the aspect of  $\langle F_U \rangle$  along the concentration of  $\text{Ag}^+$  is different from  $F_{\text{Usingle}}$  in semilogarithmic scale ( $\langle F_U \rangle$ , linear vs  $F_{\text{Usingle}}$ , sigmoidal shape). For further comparison of each shape, we equally applied the Hill equation fit from normalized  $\langle F_U \rangle$  (i.e.,  $\langle F_U^* \rangle$ ) (Figure S12A). The outcome is well fitted with Hill model ( $R^2 = 0.95$ ), which prompted us to study about the competition reaction between  $\text{H}^+$  and  $\text{Ag}^+$  within poly-C interbases (Figure S12B). The single and mean unbinding force of  $\text{Ag}^+$ -poly-C complex had different cooperativity coefficients ( $n$ ) ( $F_{\text{Usingle}}^*$ , 0.962;  $\langle F_U^* \rangle$ , 0.367) which represented the decrement of binding affinity of the binding sites between one molecule and subsequent molecules. In bulk analysis, sum of  $F_{\text{Usingle}}$  (i.e.,  $\langle F_U \rangle$ ) contains molecular heterogeneity due to various bond formations which are affected by a steric or conformational barrier, so the binding cooperativity can be decreased along with the decrease of binding affinity.<sup>71</sup>

In conclusion, we demonstrated a novel approach not only for the highly sensitive detection of  $\text{Ag}^+$  over a wide concentration range but also for statistical analysis of the interplay between  $\text{Ag}^+$ ,  $\text{H}^+$ , and the poly-C DNA duplex by intermolecular interactions measured by DEP-based force spectroscopy in a simple, robust, and high-throughput manner. Using this approach, we quantified the unbinding forces ( $F_U$ ) of the combined interactions between hydrogen and coordinate bonds in  $\text{Ag}^+$ -poly-C complexes and characterized the optimal length of poly-C DNA to sense  $\text{Ag}^+$  in distilled water (1 nM to 100  $\mu\text{M}$ ) and drinking water (1  $\mu\text{M}$  to 100  $\mu\text{M}$ ). Moreover, we also investigated the interactions of  $\text{Ag}^+/\text{H}^+$ -poly-C DNA complexes, which consist of  $\text{C}-\text{H}^+-\text{C}$  and the  $\text{C}-\text{Ag}^+-\text{C}$  duplex, using the same  $F_U$  measurement data. In this investigation, we estimated the single unbinding force and binding cooperativity of  $\text{Ag}^+$  and poly-C DNA by Poisson statistics in concert with Hill's binding model. We demonstrated that the poly-C DNA interaction without  $\text{Ag}^+$  depends on  $\text{C}-\text{H}^+-\text{C}$ , while, as the  $\text{Ag}^+$  concentration increases, the form of  $\text{C}-\text{H}^+-\text{C}$  is replaced with  $\text{C}-\text{Ag}^+-\text{C}$  with no cooperativity between  $\text{Ag}^+$  and poly-C DNA. The observations reported here demonstrate the usability and feasibility of DEPFS as a unique force spectroscopy technique, which quantifies the delicate chelation of  $\text{Ag}^+$  and polynucleotides in a disposable microfluidic chip, suggesting that a molecular mechanism can be investigated and categorized by how they interact with each other.

## ■ ASSOCIATED CONTENT

### ● Supporting Information

The Supporting Information is available free of charge on the ACS Publications website at DOI: 10.1021/acs.analchem.6b00107.

Details on supplementary experimental results and the numerical method to extract the dielectrophoretic force acting on beads that are the probe to measure the intermolecular interactions (PDF)

## ■ AUTHOR INFORMATION

### Corresponding Authors

\*E-mail: shinedew@korea.ac.kr.

\*E-mail: yusuklee@yonsei.ac.kr.

### Author Contributions

The manuscript was written through contributions of all authors. All authors have given approval to the final version of the manuscript. S.C. and G.L. contributed equally to this work.

### Notes

The authors declare no competing financial interest.

## ■ ACKNOWLEDGMENTS

This research was supported by Basic Science Research Program through the National Research Foundation of Korea (NRF) funded by the Ministry of Science, ICT & Future Planning (Grants NRF-2013R1A2A2A03005767, NRF-2013R1A1A2O53613, NRF-2015R1A1A1A05027581, and NRF-2015M3A9D7031026), Republic of Korea, and by the Yonsei University Future-Leading Research Initiative of 2015 (Grant 2015-22-0059).

## ■ REFERENCES

- (1) Alexander, J. W. *Surg. Infect.* **2009**, *10*, 289–292.
- (2) Fromm, K. M. *Nat. Chem.* **2011**, *3*, 178.
- (3) Senjen, R.; Illuminato, I. *Nano & Biocidal Silver: Extreme Germ Killers Present a Growing Threat to Public Health*; Friends of the Earth: Washington, DC, 2009.
- (4) Marambio-Jones, C.; Hoek, E. M. J. *Nanopart. Res.* **2010**, *12*, 1531–1551.
- (5) Luoma, S. N. *Silver Nanotechnologies and the Environment: Old Problems or New Challenges?*; Woodrow Wilson International Center for Scholars: Washington, DC, 2008.
- (6) Schlich, K.; Klawonn, T.; Terytze, K.; Hund-Rinke, K. *Environ. Toxicol. Chem.* **2013**, *32*, 181–188.
- (7) Navarro, E.; Piccapietra, F.; Wagner, B.; Marconi, F.; Kaegi, R.; Odzak, N.; Sigg, L.; Behra, R. *Environ. Sci. Technol.* **2008**, *42*, 8959–8964.
- (8) Garcia-Reyero, N.; Kennedy, A. J.; Escalon, B. L.; Habib, T.; Laird, J. G.; Rawat, A.; Wiseman, S.; Hecker, M.; Denslow, N.; Steevens, J. A. *Environ. Sci. Technol.* **2014**, *48*, 4546–4555.
- (9) Hossain, Z.; Huq, F. J. *Inorg. Biochem.* **2002**, *91*, 398–404.
- (10) Dadfarnia, S.; Haji Shabani, A. M.; Gohari, M. *Talanta* **2004**, *64*, 682–687.
- (11) Shamsipur, M.; Alizadeh, K.; Hosseini, M.; Caltagirone, C.; Lippolis, V. *Sens. Actuators, B* **2006**, *113*, 892–899.
- (12) Mu, H.; Gong, R.; Ren, L.; Zhong, C.; Sun, Y.; Fu, E. *Spectrochim. Acta, Part A* **2008**, *70*, 923–928.
- (13) Lin, D.-S.; Lai, J.-P.; Sun, H.; Yang, Z.; Zuo, Y. *Anal. Methods* **2014**, *6*, 1517–1522.
- (14) Ono, A.; Cao, S.; Togashi, H.; Tashiro, M.; Fujimoto, T.; Machinami, T.; Oda, S.; Miyake, Y.; Okamoto, I.; Tanaka, Y. *Chem. Commun.* **2008**, 4825–4827.
- (15) Lin, Y.-H.; Tseng, W.-L. *Chem. Commun.* **2009**, 6619–6621.
- (16) Wen, Y.; Xing, F.; He, S.; Song, S.; Wang, L.; Long, Y.; Li, D.; Fan, C. *Chem. Commun.* **2010**, 46, 2596–2598.
- (17) Li, H.; Zhai, J.; Sun, X. *Langmuir* **2011**, *27*, 4305–4308.
- (18) Yang, Y.; Li, W.; Qi, H.; Zhang, Q.; Chen, J.; Wang, Y.; Wang, B.; Wang, S.; Yu, C. *Anal. Biochem.* **2012**, *430*, 48–52.
- (19) Lin, Z.; Li, X.; Kraatz, H.-B. *Anal. Chem.* **2011**, *83*, 6896–6901.
- (20) Yan, G.; Wang, Y.; He, X.; Wang, K.; Su, J.; Chen, Z.; Qing, Z. *Talanta* **2012**, *94*, 178–183.
- (21) Zhang, Z.; Yan, J. *Sens. Actuators, B* **2014**, *202*, 1058–1064.
- (22) Park, J.; Choi, W.; Jang, K.; Na, S. *Biosens. Bioelectron.* **2013**, *41*, 471–476.
- (23) Park, J.; Lee, S.; Jang, K.; Na, S. *Biosens. Bioelectron.* **2014**, *60*, 299–304.
- (24) Clever, G. H.; Kaul, C.; Carell, T. *Angew. Chem., Int. Ed.* **2007**, *46*, 6226–6236.
- (25) Megger, D. A.; Müller, J. *Nucleosides, Nucleotides Nucleic Acids* **2010**, *29*, 27–38.
- (26) Fu, Y.; Zhang, J.; Chen, X.; Huang, T.; Duan, X.; Li, W.; Wang, J. *J. Phys. Chem. C* **2011**, *115*, 10370–10379.
- (27) Lee, S. W.; Li, H.; Bashir, R. *Appl. Phys. Lett.* **2007**, *90*, 223902.
- (28) Baek, S. H.; Chang, W.-J.; Baek, J.-Y.; Yoon, D. S.; Bashir, R.; Lee, S. W. *Anal. Chem.* **2009**, *81*, 7737–7742.
- (29) Park, I. S.; Eom, K.; Son, J.; Chang, W. J.; Park, K.; Kwon, T.; Yoon, D. S.; Bashir, R.; Lee, S. W. *ACS Nano* **2012**, *6*, 8665–8673.
- (30) Park, I. S.; Kwak, T. J.; Lee, G.; Son, M.; Choi, J. W.; Choi, S.; Nam, K.; Lee, S.-Y.; Chang, W.-J.; Eom, K.; Yoon, D. S.; Lee, S.; Bashir, R.; Lee, S. W. *ACS Nano* **2016**, *10*, 4011–4019.
- (31) Son, M.; Choi, S.; Ko, K. H.; Kim, M. H.; Lee, S.-Y.; Key, J.; Yoon, Y.-R.; Park, I. S.; Lee, S. W. *Langmuir* **2016**, *32*, 922–927.
- (32) Cheng, P.; Barrett, M. J.; Oliver, P. M.; Cetin, D.; Vezenov, D. *Lab Chip* **2011**, *11*, 4248–4259.
- (33) Cheng, P.; Oliver, P. M.; Barrett, M. J.; Vezenov, D. *Electrophoresis* **2012**, *33*, 3497–3505.
- (34) Lee, M. H.; Brass, D. A.; Morris, R.; Composto, R. J.; Ducheyne, P. *Biomaterials* **2005**, *26*, 1721–1730.
- (35) Hong, Y.; Pyo, J.-W.; Hyun Baek, S.; Woo Lee, S.; Sung Yoon, D.; No, K.; Kim, B.-M. *Opt. Lett.* **2010**, *35*, 2493–2495.
- (36) Park, I. S.; Park, S. H.; Yoon, D. S.; Lee, S. W.; Kim, B.-M. *Appl. Phys. Lett.* **2014**, *105*, 103701.
- (37) Pesce, G.; Rusciano, G.; Zito, G.; Sasso, A. *Opt. Express* **2015**, *23*, 9363–9368.
- (38) Green, N. G.; Ramos, A.; Morgan, H. J. *Phys. D: Appl. Phys.* **2000**, *33*, 632.
- (39) Holm, A. I. S.; Nielsen, L. M.; Kohler, B.; Hoffmann, S. V.; Nielsen, S. B. *Phys. Chem. Chem. Phys.* **2010**, *12*, 3426–3430.
- (40) Darwich, S.; Mougin, K.; Rao, A.; Gnecco, E.; Jayaraman, S.; Haidara, H. *Beilstein J. Nanotechnol.* **2011**, *2*, 85–98.
- (41) Lee, G.; Lee, H.; Nam, K.; Han, J.-H.; Yang, J.; Lee, S. W.; Yoon, D. S.; Eom, K.; Kwon, T. *Nanoscale Res. Lett.* **2012**, *7*, 608.
- (42) Xu, Z.; Wang, C.; Sheng, N.; Hu, G.; Zhou, Z.; Fang, H. *J. Chem. Phys.* **2016**, *144*, 014302.
- (43) Arora, K.; Prabhakar, N.; Chand, S.; Malhotra, B. D. *Sens. Actuators, B* **2007**, *126*, 655–663.
- (44) Yang, J.; Eom, K.; Lim, E.-K.; Park, J.; Kang, Y.; Yoon, D. S.; Na, S.; Koh, E. K.; Suh, J.-S.; Huh, Y.-M.; Kwon, T. Y.; Haam, S. *Langmuir* **2008**, *24*, 12112–12115.
- (45) Lee, G.; Eom, K.; Park, J.; Yang, J.; Haam, S.; Huh, Y. M.; Ryu, J. K.; Kim, N. H.; Yook, J. I.; Lee, S. W.; Yoon, D. S.; Kwon, T. *Angew. Chem., Int. Ed.* **2012**, *51*, 5837–5841.
- (46) Husale, S.; Persson, H. H. J.; Sahin, O. *Nature* **2009**, *462*, 1075–1078.
- (47) Zhang, Y.; Ge, C.; Zhu, C.; Salaita, K. *Nat. Commun.* **2014**, *5*, 5167.
- (48) Porchetta, A.; Vallée-Bélisle, A.; Plaxco, K. W.; Ricci, F. *J. Am. Chem. Soc.* **2013**, *135*, 13238–13241.
- (49) Lei, Q.-l.; Ren, C.-l.; Su, X.-h.; Ma, Y.-q. *Sci. Rep.* **2015**, *5*, 9217.
- (50) Rao, A. N.; Grainger, D. W. *Biomater. Sci.* **2014**, *2*, 436–471.
- (51) Perumalla, S. R.; Pedireddi, V. R.; Sun, C. C. *Cryst. Growth Des.* **2013**, *13*, 429–432.



- (52) Berdakin, M.; Steinmetz, V.; Maitre, P.; Pino, G. A. *J. Phys. Chem. A* **2014**, *118*, 3804–3809.
- (53) Geerts, N.; Eiser, E. *Soft Matter* **2010**, *6*, 4647–4660.
- (54) Krautbauer, R.; Rief, M.; Gaub, H. E. *Nano Lett.* **2003**, *3*, 493–496.
- (55) Marx, G. H.; Dyda, P. A.; Pethig, R. *J. Biotechnol.* **1996**, *51*, 175–180.
- (56) Krupke, R.; Hennrich, F.; Kappes, M. M.; v. Löhneysen, H. *Nano Lett.* **2004**, *4*, 1395–1399.
- (57) Dong, S.; Wang, Y. *Anal. Chim. Acta* **1988**, *212*, 341–347.
- (58) Katarina, R. K.; Takayanagi, T.; Oshima, M.; Motomizu, S. *Anal. Chim. Acta* **2006**, *558*, 246–253.
- (59) Gillingham, D.; Geigle, S.; Anatole von Lilienfeld, O. *Chem. Soc. Rev.* **2016**, *45*, 2637.
- (60) Ritchie, C. M.; Johnsen, K. R.; Kiser, J. R.; Antoku, Y.; Dickson, R. M.; Petty, J. T. *J. Phys. Chem. C* **2007**, *111*, 175–181.
- (61) Eckhardt, S.; Brunetto, P. S.; Gagnon, J.; Priebe, M.; Giese, B.; Fromm, K. M. *Chem. Rev.* **2013**, *113*, 4708–4754.
- (62) Zhao, C.; Qu, K.; Song, Y.; Xu, C.; Ren, J.; Qu, X. *Chem. - Eur. J.* **2010**, *16*, 8147–8154.
- (63) Kuriyan, J.; Konforti, B.; Wemmer, D. *The Molecules of Life: Physical and Chemical Principles*; Garland Science, Taylor & Francis Group: New York, 2012.
- (64) Jin, Y.; Wang, K.; Tan, W.; Wu, P.; Wang, Q.; Huang, H.; Huang, S.; Tang, Z.; Guo, Q. *Anal. Chem.* **2004**, *76*, 5721–5725.
- (65) Day, H. A.; Huguin, C.; Waller, Z. A. *Chem. Commun.* **2013**, *49*, 7696–7698.
- (66) Zhang, T.-b.; Zhang, C.-l.; Dong, Z.-l.; Guan, Y.-f. *Sci. Rep.* **2015**, *5*, 9143.
- (67) Berger, I.; Egli, M.; Rich, A. *Proc. Natl. Acad. Sci. U. S. A.* **1996**, *93*, 12116–12121.
- (68) Keane, P. M.; Wojdyla, M.; Doorley, G. W.; Kelly, J. M.; Parker, A. W.; Clark, I. P.; Greetham, G. M.; Towrie, M.; Magno, L. M.; Quinn, S. J. *Chem. Commun.* **2014**, *50*, 2990–2992.
- (69) Torigoe, H.; Miyakawa, Y.; Ono, A.; Kozasa, T. *Nucleosides, Nucleotides Nucleic Acids* **2011**, *30*, 149–167.
- (70) Torigoe, H.; Okamoto, I.; Dairaku, T.; Tanaka, Y.; Ono, A.; Kozasa, T. *Biochimie* **2012**, *94*, 2431–2440.
- (71) Solomatin, S. V.; Greenfeld, M.; Herschlag, D. *Nat. Struct. Mol. Biol.* **2011**, *18*, 732–734.